Ionospheric detection of gravity waves induced by tsunamis

Juliette Artru,[1] Vesna Ducic,[2] Hiroo Kanamori,[1] Philippe Lognonné[2]
and Makoto Murakami[3]

[1] *Seismological Laboratory* MC 252-21, *California Institute of Technology, Pasadena*, CA 91125, *USA. E-mail: juliette@gps.caltech.edu*
[2] *Institut de Physique du Globe de Paris, Département de Géophysique Spatiale et Planétaire,* UMR7096, 4 *avenue de Neptune,*
94107 *Saint-Maur-des-Fossés, France*
[3] *Crustal Deformation Laboratory, Geographical Survey Institute, Tsukuba, Japan*

SUMMARY

Tsunami waves propagating across long distances in the open-ocean can induce atmospheric gravity waves by dynamic coupling at the surface. In the period range 10 to 20 minutes, both have very similar horizontal velocities, while the gravity wave propagates obliquely upward with a vertical velocity of the order of $50 \, \mathrm{m \, s^{-1}}$, and reaches the ionosphere after a few hours. We use ionospheric sounding technique from Global Positioning System to image a perturbation possibly associated with a tsunami-gravity wave. The tsunami was produced after the $M_w =$ 8.2 earthquake in Peru on 2001 June 23, and it reached the coast of Japan some 22 hours later. We used data from the GEONET network in Japan to image small-scale perturbations of the Total Electron Content above Japan and up to 400 km off shore. We observed a short-scale ionospheric perturbation that presents the expected characteristics of a coupled tsunami-gravity wave. This first detection of the gravity wave induced by a tsunami opens new opportunities for the application of ionospheric imaging to offshore detection of tsunamis.

Key words: atmospheres, Global Positioning System (GPS), ionosphere, tsunamis.

GJI Seismology

1 INTRODUCTION

Tsunamis are long surface gravity waves that propagate for great distances in the ocean. They are usually triggered by submarine earthquakes, landslides or eruptions. While tide gauges can measure tsunami waves along the coast, detection and monitoring in the open ocean is very challenging due to the long wavelengths (typically 200 km) and small amplitudes (a few cm or less of sea surface vertical displacement) compared to wind-generated waves. Reported offshore detections involve ocean-bottom sensors (Hino *et al.* 2001; Tanioka 1999) (pressure gauges or seismometers), sea level measurement from Global Positioning System receivers on buoys (Gonzalez *et al.* 1998; Kato *et al.* 2000) or satellite altimetry (Okal *et al.* 1999).

Since the 1960s, numerous observations of acoustic-gravity waves in the ionosphere induced by solid Earth events, such as earthquakes, mine blasts or explosions, have been published (Bolt 1964; Harkrider 1964; Calais *et al.* 1998). They highlighted the generation of such atmospheric waves at the Earth surface by vertical displacements with very small amplitude but large wave length, such as seismic surface waves (Artru 2001; Artru *et al.* 2001). The main reason for having such coupled solid-Earth atmosphere signals is that the exponential decrease of density with height causes an exponential amplification of the atmospheric wave by conservation of the kinetic energy. In the F region of the ionosphere (150–600 km of altitude), the velocity perturbation is typically amplified by a factor

of 10^4 compared to the ground velocity, and is therefore detectable on ground-based or ground-satellite measurements (Blanc 1985).

Tsunami waves are expected to induce a similar type of coupling with the atmosphere: despite their small amplitude compared to ocean swell, they can generate atmospheric gravity waves because of their long wavelengths. The possibility of detection of tsunamis by monitoring the ionospheric signature of the induced gravity wave was proposed by Peltier & Hines (1976). They discussed the theoretical issue of the coupling, and found that the several difficulties one would expect *a priori* should not have any major consequences on the feasibility. We will recall their main conclusions in Section 2.1. To our knowledge, however, no further attempt has been performed. Part of the problem is certainly the lack of ionospheric measurements above the oceans, and also the difficulty to distinguish tsunami-related gravity waves from any other source of traveling ionospheric disturbances.

More recently, the development of high-density Global Positioning System (GPS) networks have made a breakthrough in ionospheric monitoring, allowing us to image propagation of Traveling Ionospheric Disturbances (TIDs) over large areas. Calais & Minster (1998) detected ionospheric perturbations after the 1994 Northridge earthquake. The detection and imaging of Rayleigh waves after the 2002 Denali earthquake using California GPS networks (Ducic *et al.* 2003) showed that despite the fact that GPS measures the integrated electron density between the satellite and the receiver, small scale waves could be resolved and identified using adapted data
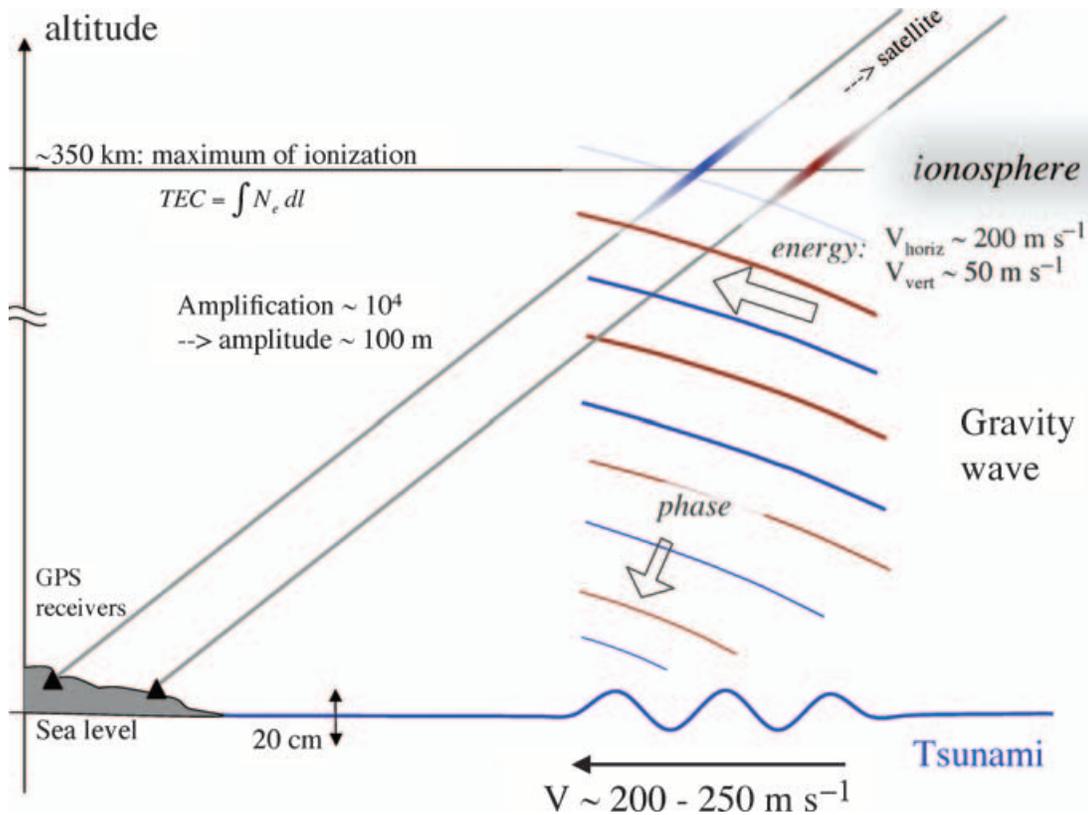
Figure 1. Schematic view of our study. The geometry of GPS measurements allows to detect ionospheric perturbations above the open ocean, and therefore possible gravity waves induced by tsunamis.

processing. Moreover, the geometry of GPS ionospheric measurements is particularly interesting for the detection of offshore signal: as the maximum of sensitivity is obtained in the F region along the satellite-receiver rays, GPS receivers on coastal areas will provide coverage off shore, up to several hundred kilometres away from the coast.

In order to study the possible existence of such ionospheric signature of tsunamis, we processed data from the continuous GPS network in Japan (GEONET) at the predicted arrival time of a tsunami generated by the Peru earthquake on 2001 June 23 ($M = 8.2$). Fig. 1 shows a schematic view of the geometry of the experiment. The data processing applied allows us to detect various TIDs propagating in the area, mostly during daytime. At the time of the tsunami arrival, however, the background activity is low. We observed a signal that has indeed the expected characteristics of a coupled tsunami-gravity waves in terms of arrival time, wave front orientation, horizontal velocity and period.

We will first recall some theoretical consideration about the coupling between tsunami and gravity waves and the motivation to select this particular event. The second part will present the data processing, similar to Ducic *et al.* (2003), applied in order to image small-scale ionospheric perturbations from the GPS data, and will describe the signal obtained. The main challenge in identifying such signal due to a tsunami-induced gravity waves is the lack of complementary measurement, both at the sea surface and in the atmosphere, that could confirm it. Indeed, gravity waves are very commonly observed in the atmosphere, and we will discuss in the last part how confidence can be built for a unique observation, as well as some of the questions still open in this observation.

2 TSUNAMI–INTERNAL GRAVITY WAVES COUPLING

The possibility of tsunami detection by the way of coupled atmospheric gravity waves has been proposed by Peltier & Hines (1976). They mainly discussed how the vertical displacement of the sea surface due to a tsunami can be a source of gravity waves in the atmosphere. The gravity wave is described using the formalism developed by Hines (1960) that we recapitulate in Appendix A. The gravity wave created at the sea surface propagates obliquely upward. Due to the exponential decrease of density with altitude, conservation of kinetic energy causes an exponential increase in the wave amplitude. As it reaches the ionosphere, the gravity wave should then perturb the local plasma, and induce some detectable signals on radio sounding. Let us quantify further the characteristics of this coupling.

2.1 Tsunami and gravity waves characteristics

Tsunami are non-dispersive waves; their propagation velocity v is obtained from shallow-water equations and depends on gravity g and water depth d as $v = \sqrt{gd}$. If we take the values $g = 9.8$ m s^{-2} and $d = 5000$ m, this velocity is $v = 221$ m s^{-1}. Typical period range is between 10 and 30 min (600–1800 s). We will use the 2-D description adopted by Peltier & Hines (1976), where the tsunami propagates as a plane wave along the x-direction. A comparison between dispersion relations for acoustic-gravity waves and tsunamis in a simple isothermal atmosphere model shows several basic properties for the expected waves.
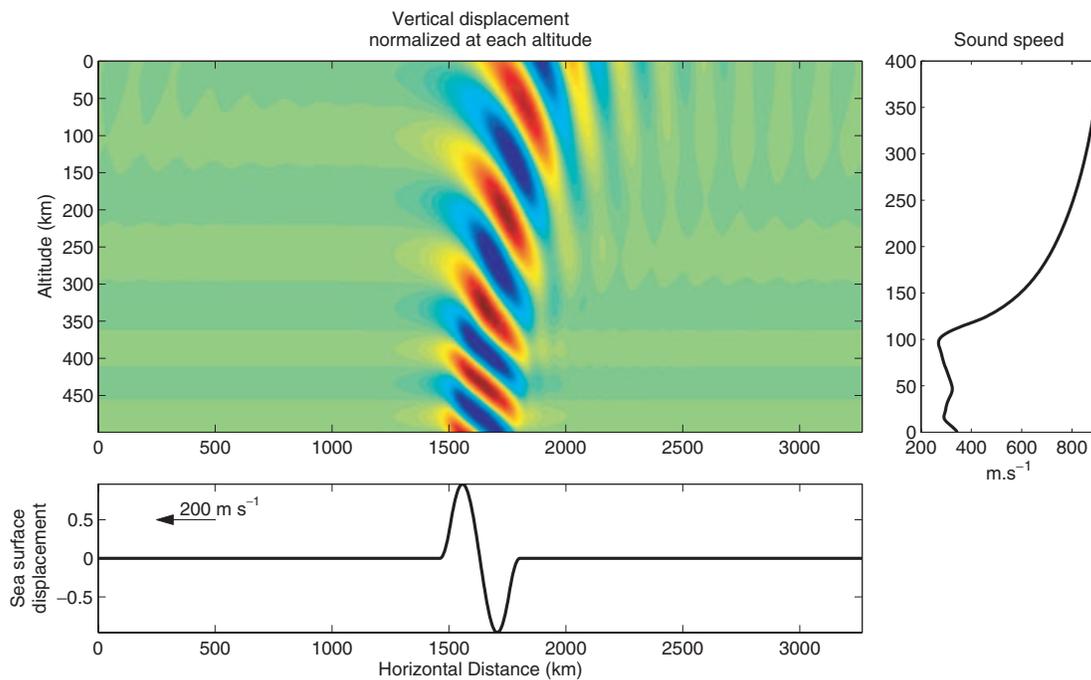
Figure 2. Numerical simulation of the gravity wave induced by a tsunami propagating at 140 m s^{-1}. The atmospheric model used is shown on the right panel, and the tsunami waveform is plotted on the bottom panel. The colour scale is normalized at each altitude to avoid saturation due to the exponential increase. At 400 km, the displacement is amplified by a factor 10^5 (this simulation neglects any attenuation mechanism).

First, the group velocity v_g of the gravity wave gives us the direction and speed of propagation of the atmospheric perturbation. For a 20-min period tsunami propagating at 221 m s^{-1}, and taking an isothermal atmosphere with a sound velocity $c = 340$ m s^{-1}, gravity acceleration $g = 9.8$ m s^{-2}, and specific heat ratio $\gamma = 1.4$, we obtain $v_{gx} = 210.5$ m s^{-1} and $v_{gz} = 43.2$ m s^{-1}. This means that the perturbation propagates horizontally at approximately the same speed as the tsunami, but will reach the ionosphere F2 peak (350 km of altitude) only after 2 hr 15 min of propagation. As the horizontal group velocity is fairly constant, there is a limited horizontal dispersion as the perturbation propagates upward, as pointed out by Peltier & Hines (1976). Fig. 2 shows a cross-section of the atmosphere perturbed by an idealized tsunami. Note that the orientation of the crest is consistent with the remarkable characteristics of gravity waves, where phase and group vertical velocities have opposite directions. We tested the effect of winds, by including in our simulation the advection terms calculated for a typical horizontal wind profile varying from 0 to 50 m s^{-1}. This did not affect significantly the outcome of the modeling, the main effect being a slight change in the geometric spreading of the wave above 100 km of altitude. Much stronger winds or large gradients may however induce a reflection of the gravity wave.

Due to the low vertical group velocity, the 'steady–state' situation described in Fig. 2 will occur only several hr after the tsunami wave was initiated. This means that some ionospheric signal might be detected only at large distances from the epicentre. Strong variations in the bathymetry, leading to changes in the tsunami speed might further alter this scenario.

2.2 Previous related observations

The mechanism described above is also responsible for the coupling between seismic surface waves and atmospheric acoustic waves.

Ionospheric oscillations induced in the wake of Rayleigh wave propagation is indeed systematically observed using ground-based Doppler sounding, for magnitudes greater than 6.5 (Artru *et al.* 2004). Some tsunami warning system was attempted using Doppler sounding between two islands in Hawaii (Najita *et al.* 1973; Najita & Yuen 1979), by the way of detection of the Rayleigh waves preceding a potentially destructive tsunami. More recently, GPS ionospheric measurements, giving access to the electron density integrated along the satellite-receiver ray, allowed us to detect perturbations after earthquakes, either emitted directly from the epicentre location, or induced by Rayleigh waves. Other related observations include explosions, mine blasts, volcanic eruptions (Calais & Minster 1998; Kanamori *et al.* 1994). In the case of short-period signals (infrasounds), successful modeling of this coupling can been performed using normal-modes (Lognonné *et al.* 1998) or ray tracing (Garcès *et al.* 1998; Virieux et al 2004).

The efficient coupling between surface motion and internal acoustic-gravity waves depends strongly on the wavelength of the signal. In particular, major energy from ocean swell may induce some infrasonic signals trapped at the base of the atmosphere (Garcès *et al.* 2003), but will not in general induce internal (i.e. upward propagating) acoustic or gravity waves in the atmosphere, because of their short wavelength range.

2.3 Gravity wave signature in the ionosphere

As the gravity waves propagates upward, it will interact with the ionospheric plasma through different mechanisms. Some early works by Yeh & Liu (1972) extended Hines's formalism to ionospheric heights, including the effect of the Lorentz force due to the magnetic field, and the ions-neutral particles collision terms. This gravity wave–ionosphere interaction is one of the main sources of Travelling Ionospheric Disturbances. TIDs are commonly observed
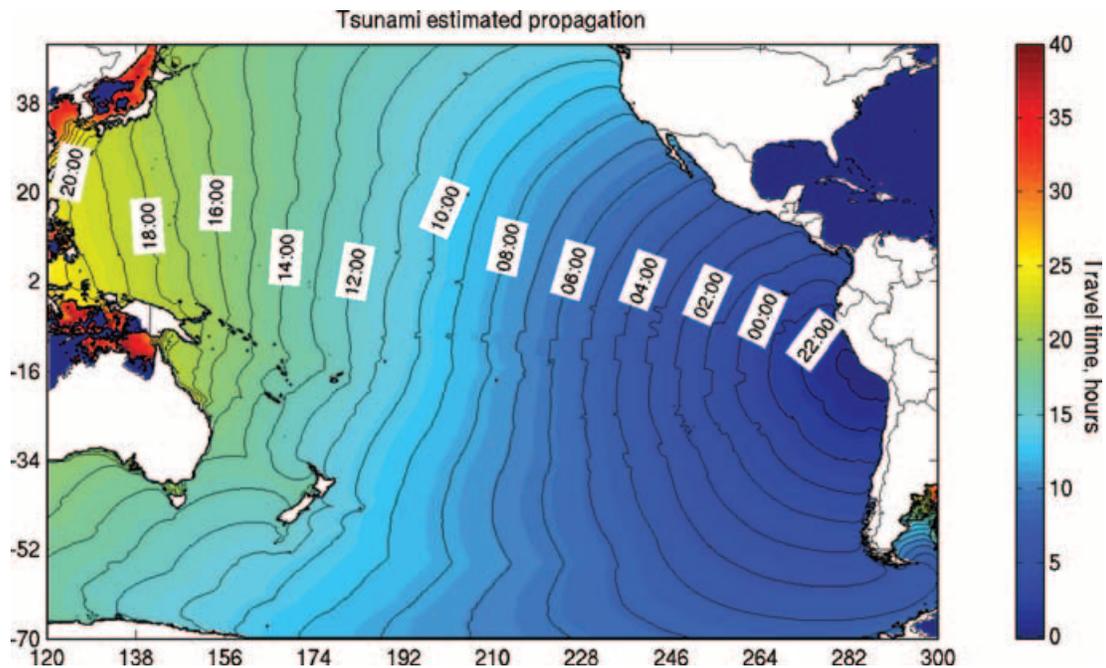
Figure 3. Estimated arrival times (ETA) for the tsunami. The contour lines show the arrival times (GMT). Courtesy of Dr Shunichi Koshimura, Disaster Reduction and Human Renovation Institution (DRI).

in the ionosphere, in a wide range of wavelength and frequency. Several studies have described the different types of TIDs usually found, and developed models of gravity waves–ionosphere coupling (Clark *et al.* 1971). However, most TIDs have periods longer than 1 hour and larger scales than what a tsunami gravity wave is likely to present.

For 30-min period waves with 2 m s^{-1} of amplitude at 180 km of altitude, Kirchengast (1996) finds that the relative perturbation in electron density can reach up to 10 per cent in the F region, with a peak between 200 and 250 km of altitude. This estimate does not seem unreasonable in our case: Considering a tsunami with a period of 30 min, an amplitude of 2 cm in the open sea, the sea surface vertical velocity is $\approx 7 \times 10^{-5}$ m s^{-1}, and if no attenuation occurs, the gravity wave amplitude at 180 km should be of the order of a few m s^{-1} by virtue of the exponential amplification.

3 OBSERVATION

3.1 Tsunami from 2001 June 23 Peru earthquake

We present here a study of the tsunami generated after the Peru earthquake on 2001 June 23 (17.41° S, 72.49° W, 20:33 GMT). This large ($M_w = 8.2$) earthquake triggered a tsunami with run-up reaching locally 2–5 m. The tsunami propagated across the Pacific Ocean and was detected on tide gauge measurements along the coast of Japan (International Tsunami Information Center 2001). Numerical simulation (Fig. 3) predict a first peak arrival there approximately 21–23 hr after the event (i.e. 17:30–19:30 GMT on June 24). The open-ocean amplitudes obtained are between 1 and 2 cm in the Northern Pacific (Koshimura 2004, personal communication). The tsunami wave was detected on tide gauges in Japan (Fig. 4) with amplitudes between 10 and 40 cm, 20 to 22 hr after the earthquake. Two dominant frequencies are apparent on the spectrograms, approximately 0.75 and 0.5 mHz, corresponding to periods of 22 and 33 min.

In these conditions, we are assured that: (1) the tsunami has been propagating for long enough to generate a gravity wave up to the ionosphere, (2) the arrival time of the tsunami on the coast of Japan is (on June 24) between 17:30 and 19:00 GMT or 02:30 to 04:00 Local Time; this the time of the day when the ionosphere is the quietest. The geomagnetic indexes for this day do not indicate any magnetic storm or unusual solar activity.

3.2 GPS ionospheric monitoring

GPS ionospheric monitoring using dense, continuous networks such as GEONET in Japan (Hatanaka *et al.* 2003) has proved to be an efficient technique to monitor small-scale perturbations (Saito *et al.* 2002; Ducic *et al.* 2003). The measured quantity is the Total Electron Content (TEC), which is the electron density integrated along the satellite-receiver ray (Mannucci 1998). Such measurement is obtained easily from the phase measurements, for each satellite–receiver couple and at each sampling time. TEC is usually expressed in TEC units (1 TECU $= 10^{16}$ e$^-$ m^{-2}), and typical diurnal variations occur in the range 10–80 TECU for a vertical ray.

For slant satellite-receiver rays, a geometric correction is needed to account for the longer path through the ionosphere, using usually the single-shell approximation: all the electron content is assumed to be at the F2 peak (altitude of maximum electron density), at about 350 km according to the International Reference Ionosphere (IRI) model; the equivalent Vertical Electron Content (VEC) is defined as VEC $=$ TEC$/\cos\theta$, where θ is the zenithal angle of the ray at 350 km. The position of the measurement is also taken at this point, called further 'piercing point'.

In order to remove diurnal variation in TEC, as well as constant receivers/satellites electronic biases we apply a high-pass filter with a cut-off at 30 min. However, this simple data processing may lead to two errors in the interpretation.

(i) First, we are now measuring perturbations of the electron content which could well be located far below or above the F2 peak. The
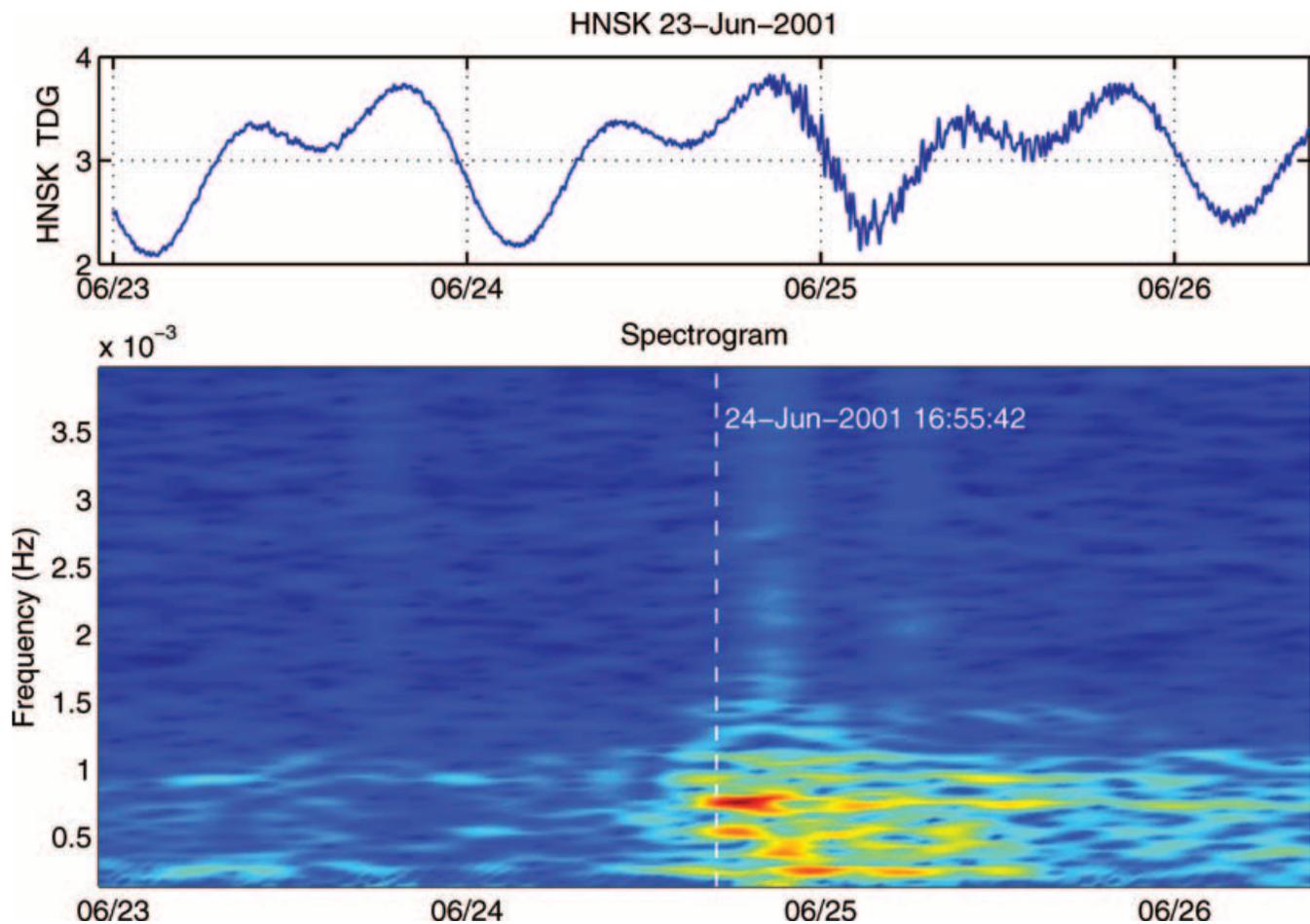
Figure 4. HNSK (Hanasaki, Hokkaido) Tide gauge time series and spectrogram. The tsunami clearly appears as short-period, small amplitudes fluctuations compared to the tidal signal. Two frequency peaks are observed, corresponding to 20 and 30 min of period.

error in the correction factor is probably negligible at this level, but the mislocation of the piercing point can be important, especially for low elevation rays. This effect can be mitigated in part by focusing our study on a single satellite at a time, where the relative location of the different measurement point is still accurate.

(ii) Secondly, as the piercing points are moving with time due to the satellite motion, some sharp static spatial variations in the TEC may appear in the time series as short period signal, and therefore would not be filtered out. Such an aliasing can however be identified *a posteriori* by looking at several receivers simultaneously.

3.3 Data processing

We processed ionospheric data from the Japanese continuous GPS network (GEONET). This network consists of more than 1000 continuous receivers, and presents a remarkable coverage of the Japan archipelago. Each receiver can usually receive signals from six or more satellites with a 30 s sampling rate, providing more than 6000 TEC measurements at each time. This data set extends 500 to 800 km offshore when a satellite is seen with a low elevation angle.

At each time, we plotted the value of the filtered TEC at the corresponding ionospheric piercing points. Traveling ionospheric disturbances can be frequently detected throughout the day, with amplitudes varying from a fraction to several TEC units, but most occur during daytime. At the estimated arrival time of the tsunami

(2–4 am in local time), a perturbation propagating towards the S-SW, with a peak-to-peak amplitude of 1 TECU, was detected along the Northeast coast of Honshu. Previous days processing did not show such perturbations of the ionosphere at that time. Fig. 5 shows such maps for several times within the window of the tsunami arrival. The orientation, wavelength and apparent velocity of the signal are at this point consistent with the expected characteristics described in Section 2.1.

4 DISCUSSION

4.1 Signal observed

Let us look at the signal observed in greater detail. Because of the possible aliasing of spatial variations of TEC into the filtered time series, a careful analysis of the geometry of the signal is needed. It is however possible to take advantage of the high density of the network to mitigate this effect. We isolated the data from one satellite–all receivers and ploted the corresponding time series as functions of time and distance from the epicentre (Fig. 6). In the ideal case of a tsunami propagating at a constant speed, the signals would have appeared along as straight line corresponding to the tsunami velocity. Here we find that the signal is indeed consistent with some velocity in the range 150–250 m s^{-1}, which is consistent with our interpretation.
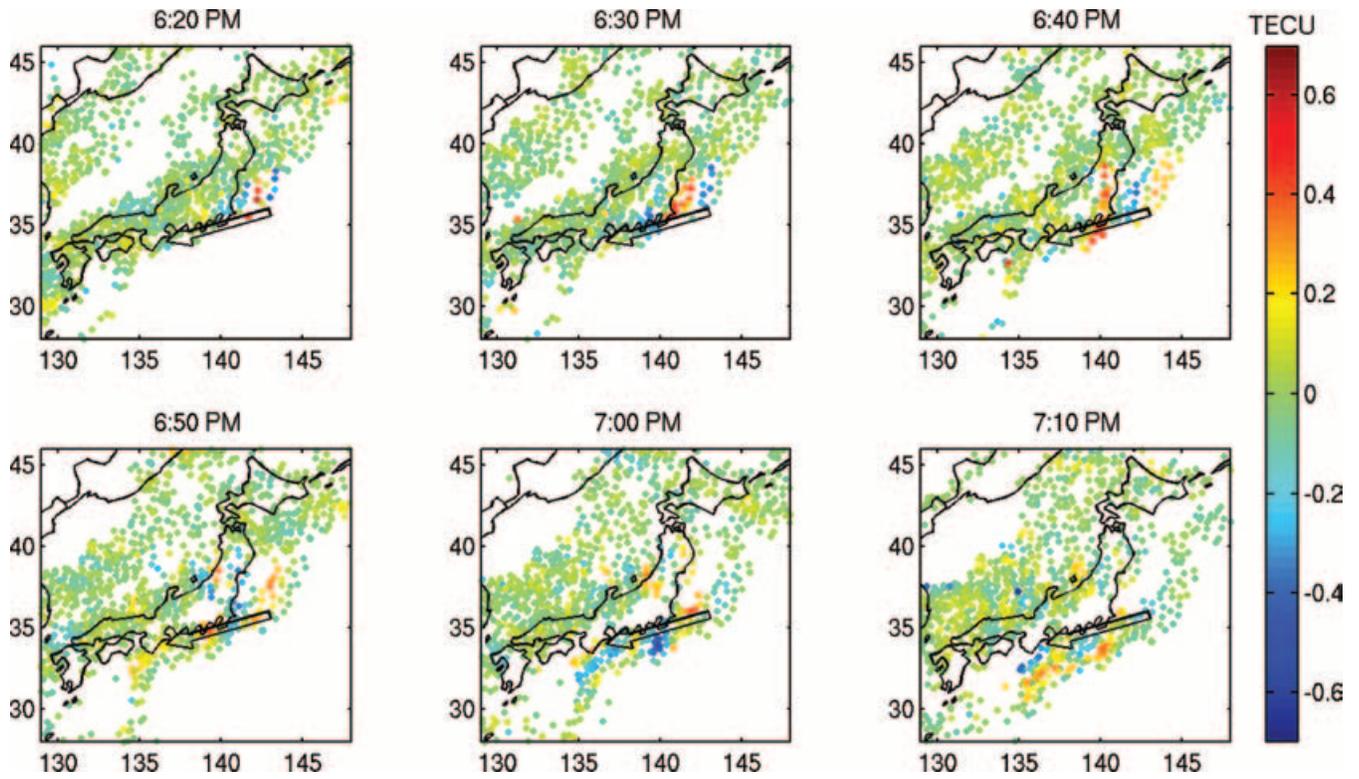
Figure 5. Observed signal: TEC variations plotted at the ionospheric piercing points. A wave-like disturbance is propagating towards the coast of Honshu. This perturbation presents the expected characteristics of a tsunami induced gravity waves, and arrives approximately at the same time as the tsunami wave itself.
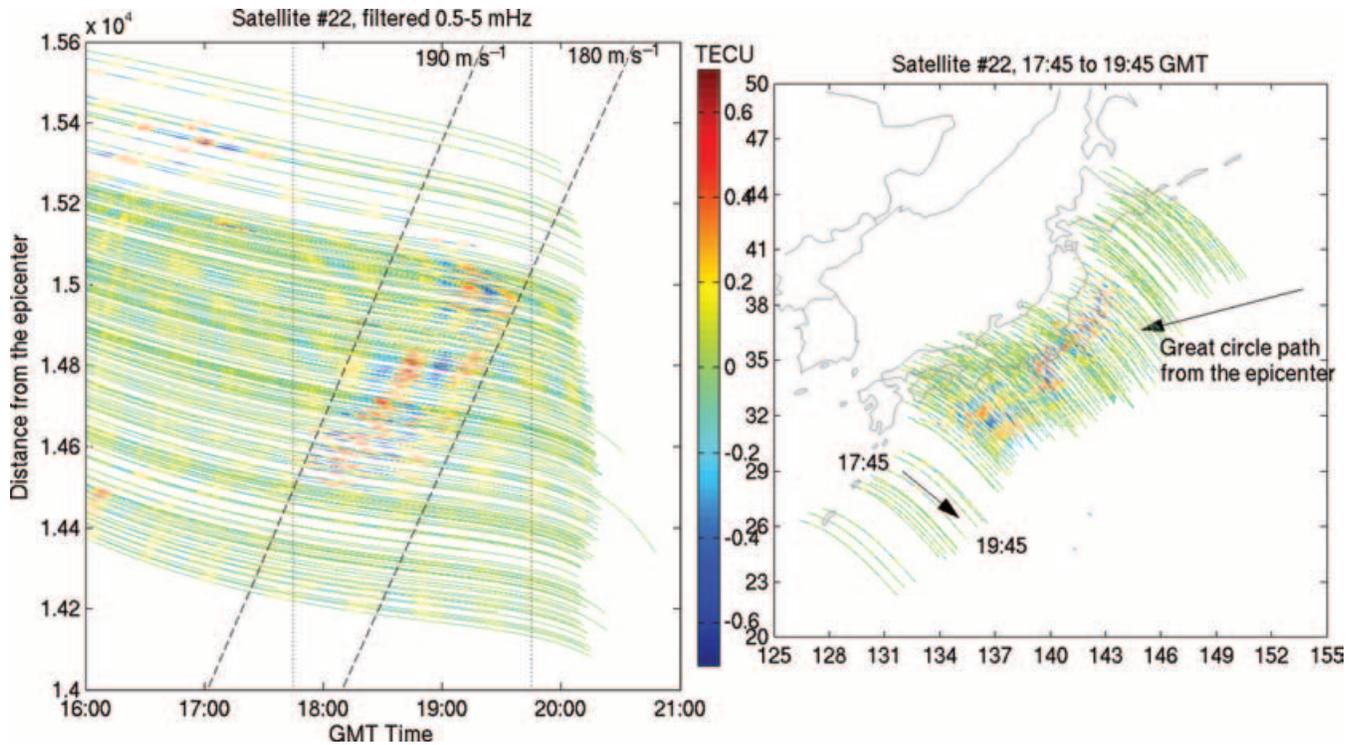
Figure 6. Time series for satellite 22 at the time of the tsunami arrival. The left panel shows the TEC variations as a function of time and distance from the epicentre (along the great circle path). The right panel shows the same time series at the moving location of the ionospheric piercing points (350 km of altitude).
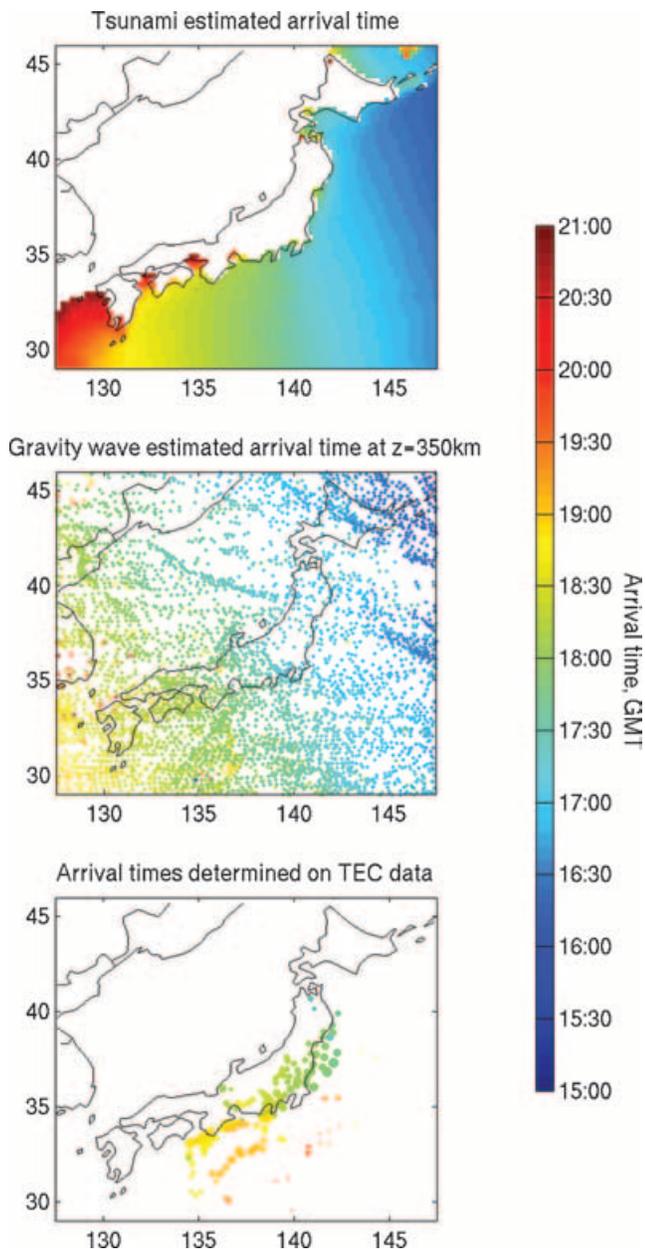
Figure 7. Tsunami arrival times (GMT) predicted and observed. The top panel is a close-up of Fig. 3 showing tsunami estimated arrival times (at sea level) in the area of study. The middle panel shows the result of the arrival time estimation, at 350 km of altitude, for the induced gravity wave. The bottom panel shows the observed arrival times, obtained by cross-correlation of all the time series from satellite 22. These travel times give an apparent horizontal velocity of between 150 and 200 m s^{-1}. The azimuth is approximately 250°.

4.2 Arrival times: observations and simulations

In a second step, we pick the arrival times of the signal on each of the time series (by cross-correlation with a reference trace). The bottom panel of Fig. 7 shows the travel times obtained. From these travel times, we can estimate the velocity and azimuth of the perturbation. We find a velocity of 150 m s^1 (±30 per cent), and an azimuth of 250°. Both are consistent with a tsunami wave propagating from the coast of Peru.

Tsunami estimated arrival (ETA) times can be calculated from the bathymetry. The arrival time map for the 2001 June 23 tsunami is

shown on Fig. 3 (Koshimura 2004, personnal communication). Using these travel times, we calculated the arrival time for the tsunami-induced gravity wave. At each point we calculated the tsunami speed from the bathymetry. Then we determined the horizontal and vertical group velocities for a 30-min period gravity wave induced by the tsunami (assuming an isothermal atmosphere in which $c = 350$ m s^{-1}). From these values and from the orientation of the tsunami wave front, we calculated the position and arrival time of the gravity wave at 350 km of altitude. The resulting arrival time map is shown on the middle panel of Fig. 7. We can compare directly those calculated arrival times with the time picks on the GPS time series (Fig. 7, lower panel). The agreement is fairly good, although the observed wave appears to be slower by 20 per cent. This is stil reasonable considering that the isothermal approximation clearly does not hold at high altitude.

4.3 Number and type of TIDS imaged with this processing

As we mentioned in Section 2.3, TIDs are a very common phenomenon, and it is very hard to determine the origin of such perturbations. It is virtually impossible to rule out some other interpretation for the origin of the signal that is the focus of our study. In order to confirm that the signal observed may indeed be related to the tsunami, we first checked that no such signal appeared in the preceding and following days. This shows that the wave is most likely not related to diurnal variations of the ionosphere. We also performed a simple count of the wave-like perturbations appearing through our data processing, with amplitudes higher than 0.1 TECU. We noted their location, time, apparent azimuth and velocity throughout 2001 June 23 and 24. The results are presented on Fig. 8. Amplitudes observed do not exceed 2.5 TECU, and as expected, daytime ionosphere presents much more TIDs than nighttime.

5 CONCLUSION

We presented here an ionospheric perturbation possibly induced by a tsunami. The detection was made off shore using Japan GEONET permanent GPS network. The signal observed is in good agreement with what is expected from theoretical considerations, and opens exciting perspectives for the study of tsunamis up to several hundred kilometres from the coastline. The fundamental features of this study and observation are as follows.

Tsunami waves are expected to couple with atmospheric gravity wave. The latter propagates obliquely upwards and interacts with the ionospheric plasma at high altitude. Noise caused by shorter wavelength sea-level perturbations (ocean swell) is filtered out in the process.

GPS ionospheric monitoring using a dense network is a powerfull tool to image small-scale perturbations of the ionosphere over large areas, in particular extending several hundred kilometres from the network location, thanks to oblique satellite-receiver rays.

The analysis for the Peru, 2001 June 23 earthquake and tsunami showed indeed a signal with the expected characteristics. The sea level displacement for this tsunami wave is of the order of 1–2 cm, and the amplitude of the ionospheric perturbation is ±1 TECU. This amplitude is similar to most of the TIDs observed during that day; however, a larger tsunami would be expected to produce ionospheric perturbations larger than this background activity.

This is so far a unique observation, that will need to be confirmed both on future tsunami occurences, and through a better understanding of the coupling mechanism. In particular several difficulties in
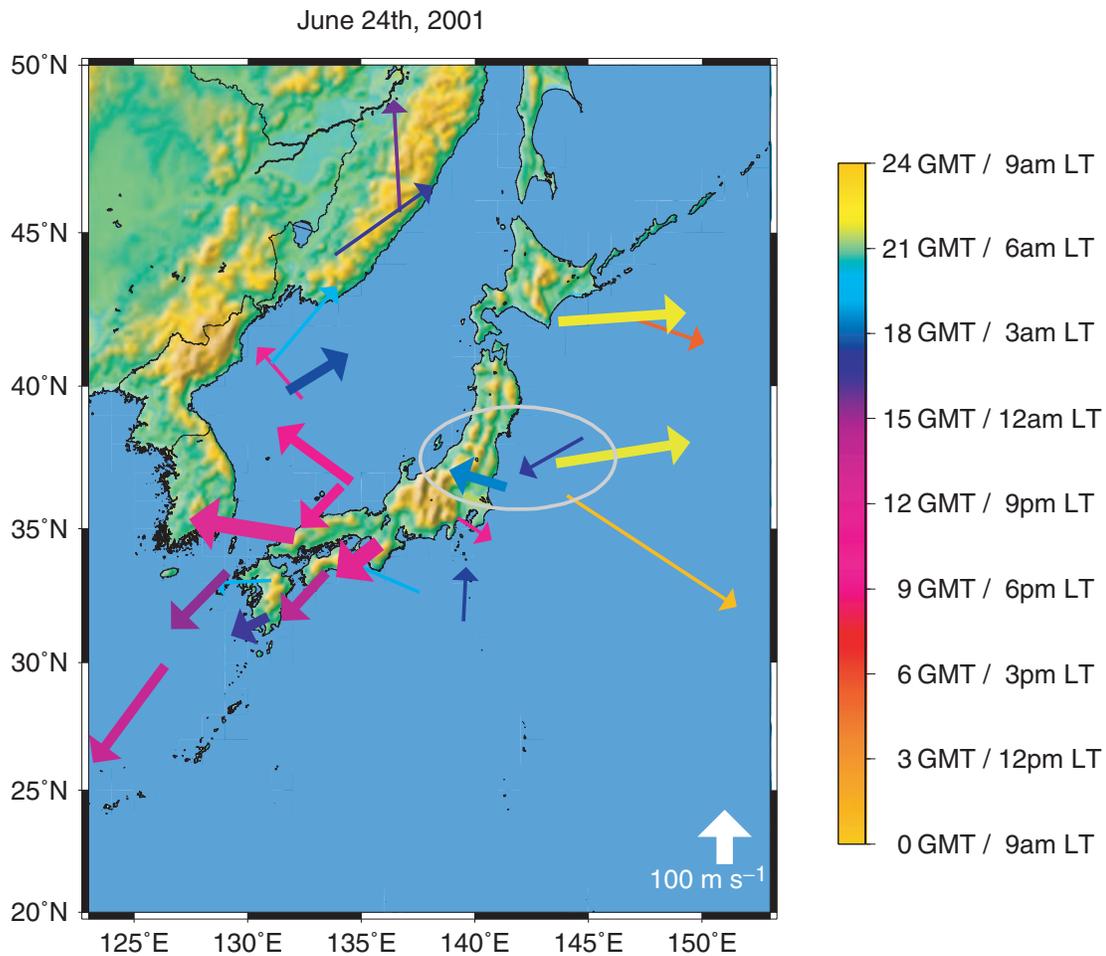
Figure 8. Waves observed on filtered TEC maps throughout 2001 June 24. The thickness of the arrows indicate the approximate amplitude of the wave (lower than 0.75 TECU, between 0.75 and 1.5 TECU, and between 1.5 and 2.25 TECU). The direction is the azimuth, and the lenght is proportional to the speed. Finally, the colour indicate the time of observation (reddish colours are the local day time, blue is nighttime). The ellipse shows the possible tsunami signal.

the description of the atmospheric–ionospheric perturbation have to be addressed, e.g. reflection in the atmosphere, attenuation, efficiency of the gravity wave–ionosphere coupling, dispersion of the signal. However, the perspectives for this work are very exciting, as tsunami waves are extremely difficult to observe in the open ocean: the associated gravity waves in the upper atmosphere might prove to be a valuable signature.

REFERENCES

Artru, J., 2001. Ground-based or satellite observations and modeling of post-seismic ionospheric signals, *PhD thesis,* Institut de Physique du Globe de Paris (in French).

Artru, J., Lognonné, P. & Blanc, E., 2001. Normal modes modelling of post-seismic ionospheric oscillations, *Geophys. Res. Lett.,* **28**(4), 697–700.

Artru, J., Farges, T. & Lognonné, P., 2004. Acoustic waves generated from seismic surface waves: propagation properties determined from Doppler sounding observation and normal-mode modeling, *Geophys. J. Int.,* **158,** 1067–1077 (doi: 10.1111/j.1365-246X.2004.02377.x).

Blanc, E., 1985. Observations in the upper atmosphere of infrasonic waves from natural or artificial sources: A summary, *Ann. Geophys.,***3**(6), 673–688.

Bolt, B.A., 1964. Seismic air waves from the great 1964 Alaska earthquake, *Nature,* **202**(4937), 1095–1096.

Calais, E. & Minster, J.B., 1995. GPS detection of ionospheric perturbations following the January 17, 1994, Northridge earthquake, *Geophys. Res. Lett.,* **22**(9), 1045–1048.

Calais, E. & Minster, J.B., 1998. GPS, earthquakes, the ionosphere, and the space shuttle, *Phys. Earth planet. Inter.,* **105,** 167–181.

Calais, E., Minster, J.B., Hofton, M.A. & Hedlin, M.A.H., 1998. Ionospheric signature of surface mine blasts from global positioning system measurements, *Geophys. J. Int.,* **132**(1), 191–202.

Clark, R.M., Yeh, K.C. & Liu, C.H., 1971. Interaction of internal gravity waves with the ionospheric f2-layer, *Phys. Earth planet. Inter.,* **33,** 1567–1576.

Ducic, V., Artru, J. & Lognonné, P., 2003. Ionospheric remote sensing of the denali earthquake rayleigh surface waves, *Geophys. Res. Lett.,* **30**(18), 1951–1954, doi:10.1029/2003GL017,812.

Garcès, M., Hansen, R. & Lindquist, K., 1998. Traveltimes for infrasonic waves propagating in a stratified atmosphere, *Geophys. J. Int.*, **135**, 255–263.

Garcès, M., Hetzer, C., Merrifield, M., Willis, M. & Aucan, J., 2003. Observations of surf infrasound in Hawai'i, *Geophys. Res. Lett.*, **30**(24), 2264–2267, doi: 10.1029/2003GL018,614.

Gonzalez, F.I., Milburn, H.M., Bernard, E.N. & Newman, J.C., 1998. Deep-ocean assessment and reporting of tsunamis (dart): Brief overview and status report, in *Proceedings of the International Workshop on Tsunami Disaster Mitigation, 19–22 January 1998,* Tokyo, Japan.

Harkrider, D.G., 1964. Theoretical and observed acoustic-gravity waves from explosive sources in the atmosphere, *J. geophys. Res.,* **69,** 5295.

Hatanaka, Y., Iizuka, T., Sawada, M., Yamagiwa, A., Kikuta, Y., Johnson, J.M. & Rocken, C., 2003. Improvement of the analysis strategy of GEONET, *Bull. Geogr. Surv. Inst.*, **49,** 11–37.

Hines, C.O., 1960. Internal atmospheric gravity waves at ionospheric heights, *Canadian J. of Phys.*, **38,** 1441–1481.

Hino, R., Tanioka, Y., Kanazawa, T., Sakai, S., Nishino, M. & Suyehiro, K., 2001. Micro-tsunami from a local interplate earthquake detected by cabled offshore tsunami observation in northeastern japan, *Geophys. Res. Lett.,* **28**(18), 3533–3536.

International Tsunami Information Center–ITIC, 2001. 23–24 june 2001 20:33 GMT–Peruvian earthquake and tsunami, http://www.prh.noaa.gov/itic.

Kanamori, H., Mori, J. & Harkrider, D.G., 1994. Excitation of atmospheric oscillations by volcanic eruptions, *J. geophys. Res.,* **22,** 21947–21961.

Kato, T., Terada, Y., Kinoshita, M., Kakimoto, H., Isshiki, H., Matsuishi, M., Yokoyama, A. & Tanno, T., 2000. Real-time observation of tsunami by rtk-gps, *Earth Planet Space,* **52**(10), 841–845.

Kirchengast, G., 1996. Elucidation of the physics of the gravity wave-tid relationship with the aid of theoretical simulations, *J. geophys. Res.,* **101**(A6), 13 353–13 368.

Lognonné, P., Clévédé, E. & Kanamori, H., 1998. Computation of seismograms and atmospheric oscillations by normal-mode summation for a spherical earth model with realistic atmosphere, *Geophys. J. Int.,* **135**(2), 388–406.

Mannucci, A.J., 1998. A global mapping technique for gps-derived ionospheric electron content measurements, *Radio Science,* **33,** 565–582.

Najita, K., Weaver, P.F. & Yuen, P.C., 1973. A tsunami warning system using an ionospheric technique, *Proceedings of the IEEE,* **62**(5), 563–567.

Najita, K. & Yuen, P.C., 1979. Long-Period Oceanic Rayleigh Wave Group Velocity Dispersion Curve From HF Doppler Sounding of the Ionosphere, *J. geophys. Res.,* **84**(A4), 1253–1260.

Okal, E.A., Piatanesi, A. & Heinrich, P., 1999. Tsunami detection by satellite altimetry, *J. geophys. Res.,* **104**(B1), 599–615.

Peltier, W.R. & Hines, C.O., 1976. On the possible detection of tsunamis by a monitoring of the ionosphere, *J. geophys. Res.,* **81**(12), 1995–2000.

Saito, A., Nishimura, M., Yamamoto, M., Fukao, S., Tsugawa, T., Otsuka, Y., Miyazaki, S. & Kelley, M.C., 2002. Observations of traveling ionospheric disturbances and 3-m scale irregularitires in the nighttime f-region ionosphere with the mu radar and gps network, *Earth Planet Space,* **54,** 31–44.

Tanioka, Y., 1999. Analysis of the far-field tsunamis generated by the 1998 Papua New Guinea earthquake, *Geophys. Res. Lett.,* **26**(22), 3393–3396.

Virieux, J., Garnier, N., Blanc, E. & Dessa, J.-X., 2004. Paraxial ray tracing for atmospheric wave propagation, *Geophys. Res. Lett.,* **31**(20), L20105, doi:10.1029/2004 GL 020514.

Yeh, K.C. & Liu, C.H., 1972. *Theory of ionospheric waves* 402–418 pp., New York, Academic Press.

APPENDIX A: ACOUSTIC-GRAVITY WAVES

Hines (1960) established a convenient description of acoustic-gravity waves in an inviscid, isothermal atmosphere. The equations of motion are:

$$\text{Continuity}: \frac{\partial \rho}{\partial t} + \mathbf{v} \cdot \nabla \rho = -\rho \nabla \cdot \mathbf{v}$$

$$\text{Momentum}: \frac{\partial \mathbf{v}}{\partial t} + \mathbf{v} \cdot \nabla \mathbf{v} = \mathbf{g} - \frac{1}{\rho} \nabla p$$

$$\text{Adiabaticity}: \frac{\partial p}{\partial t} + \mathbf{v} \cdot \nabla p = C_s^2 \left(\frac{\partial \rho}{\partial t} + \mathbf{v} \cdot \nabla p \right)$$

where ρ is the density, p is the pressure, $\mathbf{v}$ is the neutral gas velocity, $\mathbf{g}$ is the acceleration due to gravity and C_s is the constant sound speed. In the equilibrium state, $\mathbf{v}_0 = 0$ and both ρ_0 and p_0 are proportional to $\exp(z/2H)$, where $H = C_s^2/\gamma \mathbf{g}$ is the density scale height, γ being the specific heat ratio. Assuming ρ_1, p_1, and $\mathbf{v}$ are small perturbations with no dependency along the *y*-axis, we may solve the linearized equations to obtain harmonic solutions with ρ_1/ρ_0, p_1/p_0 and $\mathbf{v}$ proportional to $\exp[i(\omega t - k_x x - k_z z)]$. If we define $k_z' = k_z + i/2H$, the following dispersion relation may be derived:

$$\omega^4 - \omega^2 C_s^2 \left(k_x^2 + k_z'^2 \right) + (\gamma - 1)g^2 k_x^2 - \gamma^2 g^2 \omega^2 / 4C_s^2 \qquad \text{(A1)}$$

Propagating solutions, with k_z' real, exist for two frequency ranges: acoustic modes ($\omega > \omega_a = \gamma g/2C_s$) are governed primarily by compression whereas gravity modes ($\omega < \omega_g = (\gamma - 1)^{1/2}g/C_s$) are governed primarily by buoyancy (ω_g is the Brunt-Väisälä frequency). Typically $\omega_a/2\pi = 3.3$ mHz and $\omega_g/2\pi = 2.9$ mHz in the lower atmosphere. The scale height H drives the exponential increase of the amplitude with altitude.